

Buoyancy-induced time delays in Babcock-Leighton flux-transport dynamo models

L. Jouve, M. R. E. Proctor, and G. Lesur

DAMTP, Wilberforce Road, CB3 0WA Cambridge, UK
e-mail: lj272@damtp.cam.ac.uk

Received 18 March 2010 / Accepted 19 May 2010

ABSTRACT

Context. The Sun is a magnetic star whose cyclic activity is thought to be linked to internal dynamo mechanisms. A combination of numerical modelling with various levels of complexity is an efficient and accurate tool to investigate such intricate dynamical processes.

Aims. We investigate the role of the magnetic buoyancy process in 2D Babcock-Leighton dynamo models, by modelling more accurately the surface source term for poloidal field.

Methods. To do so, we reintroduce in mean-field models the results of full 3D MHD calculations of the non-linear evolution of a rising flux tube in a convective shell. More specifically, the Babcock-Leighton source term is modified to take into account the delay introduced by the rise time of the toroidal structures from the base of the convection zone to the solar surface.

Results. We find that the time delays introduced in the equations produce large temporal modulation of the cycle amplitude even when strong and thus rapidly rising flux tubes are considered. Aperiodic modulations of the solar cycle appear after a sequence of period doubling bifurcations typical of non-linear systems. The strong effects introduced even by small delays is found to be due to the dependence of the delays on the magnetic field strength at the base of the convection zone, the modulation being much less when time delays remain constant. We do not find any significant influence on the cycle period except when the delays are made artificially strong.

Conclusions. A possible new origin of the solar cycle variability is here revealed. This modulated activity and the resulting butterfly diagram are then more compatible with observations than what the standard Babcock-Leighton model produces.

Key words. methods: numerical – Sun: dynamo – Sun: activity – Sun: interior – magnetic fields

1. Introduction

Our Sun is a prime example of a very turbulent and magnetically active star. Its robust 22-yr activity cycle originates in the periodic polarity reversal of the Sun's internal large-scale magnetic field. As a result, sunspots emerge at the solar surface with statistically well-defined dynamical and morphological characteristics. These sunspots are thought to be the surface manifestations of strong toroidal magnetic structures created at the base of the convection zone and which rise through the plasma under the effect of magnetic buoyancy (Parker 1955). This toroidal field undergoes cyclic variations along with the poloidal field, which flips polarity at sunspot cycle maxima. Even if a robust regular activity is easily exhibited in the Sun, a significant modulation of both the amplitude and the frequency of the cycle has been observed. In particular, periods of strongly reduced activity have been revealed, the most famous being the Maunder minimum between 1650 and 1700, during when no sunspots were to be seen at the solar surface (Eddy 1976). Today, understanding the origins of such a variability has become crucial. Not only is the impact on satellites, astronauts, power grids or radio communications significant but the climatologists community now tends to address more and more the question of the influence of solar variability on the Earth climate (e.g. Bard & Frank 2006; Lean 2005).

The classical explanation for the cyclic activity of the large-scale magnetic field is that a dynamo process acts in the solar interior to regenerate the three components of the magnetic field and sustain them against ohmic dissipation. The inductive action

of the complex fluid motions would thus be responsible for the vigorous regeneration of magnetic fields and for its non-linear evolution in the solar interior (see Charbonneau 2005; Miesch 2005, for recent reviews on the subject).

Understanding how these complex physical processes operating in the solar turbulent plasma non-linearly interact is very challenging. One successful and powerful approach is to rely on multi-dimensional magnetohydrodynamic (MHD) simulations. In this context, two types of numerical experiments have been performed since the 70's: kinematic mean-field axisymmetric dynamo models which solve only the mean induction equation (Steenbeck & Krause 1969; Roberts 1972; Stix 1976; Krause & Raedler 1980) and full 3D global models which explicitly solve the full set of MHD equations (Gilman 1983; Glatzmaier 1985; Cattaneo 1999; Brun et al. 2004). Those two approaches are complementary and needed since 2D mean-field models are limited by the fact that they rely on simplified descriptions of complex physical processes such as turbulence and since the cost of 3D models makes it difficult, as of today, to provide any reliable predictions concerning the large-scale magnetic cycle.

As far as the first kind of numerical simulations is concerned, a particular model has been favoured by a part of the community, namely the Babcock-Leighton flux-transport model first proposed by Babcock (1961) and Leighton (1969). This model has proved to be very efficient at reproducing several properties of the solar cycle as the equatorward branch of activity or the phase relationship between toroidal and poloidal fields. It has thus been extensively used since the 90's (Wang & Sheeley 1991; Durney 1995; Dikpati & Charbonneau 1999;

Nandy & Choudhuri 2001), even to make tentative predictions of the next solar cycle (Dikpati & Gilman 2006). In this formulation, the poloidal field owes its origin to the tilt of active regions emerging at the Sun’s surface at various latitudes during the solar cycle. It thus relies on a different mechanism than “classical” $\alpha\Omega$ dynamo models for which the poloidal field is generated by turbulent helical motions twisting and shearing toroidal field lines inside the convection zone. The emergence of tilted active regions at the photosphere is the result of the complex non-linear evolution of strong toroidal structures from the base of the convection zone (CZ), where they are created through the Ω -effect. It is thus natural to rely on 3D MHD simulations of rising toroidal structures in the convection zone to gain some insight on the best way to model the Babcock-Leighton source term.

Many models carried out since the 80’s relied on the assumption that toroidal flux is organised in the form of discrete flux tubes which will rise cohesively from the base of the CZ up to the solar surface. These models enabled to demonstrate that the initial strength of magnetic field was an important parameter in the evolution of the tube and that the active regions tilts could be explained by the action of the Coriolis force on the magnetic structure (D’Silva & Choudhuri 1993; Fan et al. 1994; Caligari et al. 1995). More sophisticated multidimensional models were then developed and extended to the upper part of the CZ and the transition to the solar atmosphere (Magara 2004; Archontis et al. 2005; Cheung et al. 2007; Martinez et al. 2008). Computations were then performed to study the influence of convective turbulent flows on the dynamical evolution of flux ropes inside the CZ (Dorch et al. 2001; Cline 2003; Fan et al. 2003; Jouve & Brun 2009). In particular in Jouve & Brun (2009), such computations were made in a global spherical geometry and thus allowed to assess the combined role of hoop stresses, Coriolis force, convective plumes, turbulence, mean flows and sphericity on the tube evolution and on the subsequent emerging regions, along with the usual parameters such as field strength, twist of the field lines or magnetic diffusion. How can the results of 3D simulations of this presumed major step of the dynamo loop be reintroduced in 2D mean-field models? This is the question we are addressing in this work. A particular point we retain from these simulations is that the rise velocity and thus the rise time of magnetic structures is strongly dependent on the initial field strength at the base of the convection zone. Indeed, magnetic buoyancy competes with convective flows to control the trajectory and the speed of the flux tubes while they rise. Since the Babcock-Leighton source term relies on this process to regenerate poloidal fields, it may be worth trying to introduce magnetic-field dependent time delays caused by rising toroidal fields in those models and analyze the influence on the solar cycle.

Indeed, time delays built up in solar dynamo models have been shown to cause long-term modulation of the dynamo cycle and under some circumstances to lead to a chaotic behaviour (Yoshimura 1978; Charbonneau et al. 2005; or Wilmot-Smith et al. 2006). In the framework of mean-field dynamo theory, several possibilities have been studied to explain the variability of the solar cycle. They mainly fell into two categories: stochastic forcing or dynamical nonlinearities. Indeed, as we mentioned above, the solar convection zone is highly turbulent and it would be surprising if the dynamo processes acting inside this turbulent plasma were nicely regular. The influence of stochastic fluctuations in the mean-field dynamo coefficients has been studied in various models (e.g. Hoyng 1988; Ossendrijver & Hoyng 1996; Weiss & Tobias 2000; Charbonneau & Dikpati 2000). Moreover, the dynamical

feedback of the strong dynamo-generated magnetic fields is likely to be significant enough to produce non-linear effects on the activity cycle. A number of models have introduced these non-linear effects (Proctor 1977; Tobias 1997; Moss & Brooke 2000; Bushby 2006; Rempel 2006) and have resulted in the production of grand minima-like periods or other strong modulation of the cyclic activity. However, time delays have hardly been considered and if they were, they were mainly due to the advection time by meridional flow. Indeed, the time-scale of the buoyant rise of flux tubes was considered to be so small compared to the cycle period (and to the meridional flow turnover time) that this particular step was assumed to be instantaneous. However, we would like to address the question of the influence of magnetic field dependent delays on the cycle produced by Babcock-Leighton models and especially on its potential modulation. We propose to do so in the present paper.

This article is organized as follows: Sect. 2 summarizes the results of 3D calculations which will be used in our modified 2D mean-field Babcock-Leighton model. The formulation of this new model is then presented, with a particular focus on the modification of the surface source term. Results of 2D models are shown in Sect. 4 and analyzed in the following two sections. Sections 5 and 6 present and study the behaviour of a reduced set of ordinary differential equations designed to gain some insight on the results of the 2D model. We discuss the results and conclude in Sect. 7.

2. Summary of the 3D calculations

In this section, we briefly summarize the results obtained by Jouve & Brun (2009). They use 3D simulations in a rotating spherical convective shell to compute the non-linear evolution of a magnetic flux tube inside the turbulent convection zone.

2.1. Model and background

The computations presented in Jouve & Brun (2009) use the ASH code which solves the anelastic equations of magneto-hydrodynamics in three dimensions and in spherical geometry Clune et al. (1999; Miesch et al. 2000; Brun et al. 2004). The first step of these calculations is to trigger the convective instability in the rotating sphere and let the model evolve until it reaches a statistically steady state. A twisted magnetic flux tube is then introduced at the base of the modelled convection zone, in entropy and pressure equilibrium. The lack of mechanical equilibrium thus causes the tube to be initially buoyant and rise through the convection zone up to the top of the computational domain. In this work, the interactions between the magnetic tube-like structure and convective motions were investigated for different initial field strength and these results were compared to isentropic cases (where the convective instability is not triggered). We do not go into the details of the simulations and the results. We just wish to summarise some of the findings of these 3D calculations which will be useful for the present work.

2.2. The rise velocity

As shown in Jouve & Brun (2009), while it rises, the flux tube creates its own local velocity field which may strongly disturb the background velocity field, especially when the initial magnetic field intensity is strong compared to that of the equipartition field B_{eq} (defined as the field which energy is equal to the kinetic energy of the strongest downdrafts). This explains why

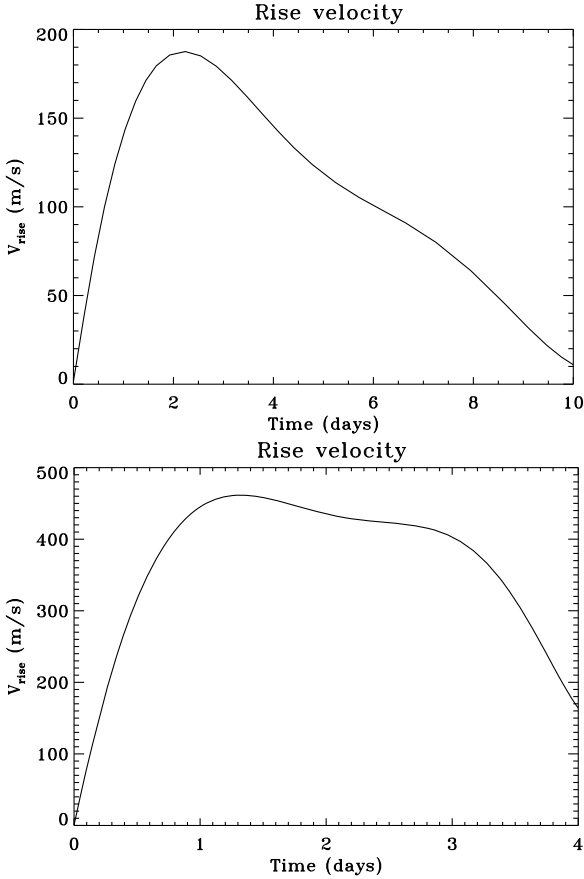


Fig. 1. Rise velocity of tubes introduced at $5 B_{\text{eq}}$ (upper panel) and $10 B_{\text{eq}}$ (lower panel) measured as a function of time during the evolution of the tubes from the base of the CZ up to about $0.9 R_{\odot}$.

the tube is more or less influenced by the convective motions as it evolves in the CZ. Indeed, if the initial magnetic field on the axis of the rope is 6×10^5 G (corresponding to $10 B_{\text{eq}}$), the tube creates a velocity through the action of the Lorentz force which dominates against the background velocity. Since a strong up-flow is thus created near the tube axis, the rising mechanism is very efficient and the tube reaches the top of the CZ in only 3 to 4 days. In the weaker case (where the initial field strength is 3×10^5 G, corresponding to $5 B_{\text{eq}}$), the velocity field created by the magnetic structure is comparable to the background velocity field and the latter is thus able to influence the behaviour of the flux rope as it rises, the rise time is in this case of about 12 days.

Figure 1 shows more precisely the evolution of the rise velocity of tubes introduced at the two different field strengths discussed above. On the upper panel, the rise velocity for the $5 B_{\text{eq}}$ -field is shown and the lower panel shows the evolution for the stronger field ($10 B_{\text{eq}}$). We first note the different time scales for the tubes to reach the surface, and this is the particular feature which will be introduced in 2D mean-field models. This figure also shows that the acceleration phase of these two tubes are similar, but after the maximal velocity has been reached, the behaviour of the two tubes differs. In particular, the weak tube gets strongly influenced by the convective motions and magnetic diffusion. As a consequence, its rise velocity is significantly reduced as it proceeds through the convection zone. On the contrary, after the strong tube has reached its maximal velocity, it keeps making its way to the surface at the same speed and the strong decrease shown on the figure is eventually strongly linked to the upper boundary condition (the boundary conditions for the velocity are stress-free and impenetrable in this case).

3. Reintroduction in 2D models

The idea of this work is to design a new 2D mean-field flux transport Babcock-Leighton model which takes into account the findings of 3D calculations concerning the rise of strong toroidal structures from the base of the convection zone up to the surface. In this section, we thus present the usual mean-field equations and the basic ingredients used in the model, with a particular focus on the new Babcock-Leighton surface source term.

3.1. The mean field Babcock-Leighton model

To model the solar global dynamo, we use the hydromagnetic induction equation, governing the evolution of the magnetic field \mathbf{B} in response to advection by a flow field \mathbf{V} and resistive dissipation.

$$\frac{\partial \mathbf{B}}{\partial t} = \nabla \times (\mathbf{V} \times \mathbf{B}) - \nabla \times (\eta \nabla \times \mathbf{B}), \quad (1)$$

where η is the magnetic diffusivity.

As we are working in the framework of mean-field theory, we express both magnetic and velocity fields as a sum of large-scale (that will correspond to mean field) and small-scale (associated with fluid turbulence) contributions. Averaging over some suitably chosen intermediate scale makes it possible to write two distinct induction equations for the mean and the fluctuating parts of the magnetic field. A closure relation is then used to express the electromotive force in terms of mean magnetic field, leading to a simplified mean-field equation. In this work we will replace the emf by a surface Babcock-Leighton term (Babcock 1961; Leighton 1969; Wang et al. 1991; Dikpati & Charbonneau 1999; Jouve & Brun 2007a) as described in details below.

We work here in spherical geometry and under the assumption of axisymmetry. Reintroducing a poloidal/toroidal decomposition of the magnetic and velocity fields in the mean induction equation, we get two coupled partial differential equations, one involving the poloidal potential A_{ϕ} and the other concerning the toroidal field B_{ϕ} .

$$\frac{\partial A_{\phi}}{\partial t} = \frac{\eta}{\eta_t} \left(\nabla^2 - \frac{1}{\varpi^2} \right) A_{\phi} - R_e \frac{\mathbf{v}_p}{\varpi} \cdot \nabla (\varpi A_{\phi}) + C_s S(r, \theta, B_{\phi}) \quad (2)$$

$$\frac{\partial B_{\phi}}{\partial t} = \frac{\eta}{\eta_t} \left(\nabla^2 - \frac{1}{\varpi^2} \right) B_{\phi} + \frac{1}{\varpi} \frac{\partial (\varpi B_{\phi})}{\partial r} \frac{\partial (\eta / \eta_t)}{\partial r} - R_e \varpi \mathbf{v}_p \cdot \nabla \left(\frac{B_{\phi}}{\varpi} \right) - R_e B_{\phi} \nabla \cdot \mathbf{v}_p + C_{\Omega} \varpi (\nabla \times (\varpi A_{\phi} \hat{\mathbf{e}}_{\phi})) \cdot \nabla \Omega, \quad (3)$$

where $\varpi = r \sin \theta$, η_t is the turbulent magnetic diffusivity (diffusivity in the convective zone), \mathbf{v}_p the flow in the meridional plane (i.e. the meridional circulation), Ω the differential rotation, $S(r, \theta, B_{\phi})$ the Babcock-Leighton source term for poloidal field. In order to write these equations in a dimensionless form, we choose as length scale the solar radius (R_{\odot}) and as time scale the diffusion time (R_{\odot}^2 / η_t) based on the envelope diffusivity (η_t). This leads to the appearance of three control parameters $C_{\Omega} = \Omega_0 R_{\odot}^2 / \eta_t$, $C_s = s_0 R_{\odot} / \eta_t$ and $R_e = v_0 R_{\odot} / \eta_t$ where Ω_0 , s_0 , v_0 are respectively the rotation rate and the typical amplitude of the surface source term and of the meridional flow.

Equations (2) and (3) are solved in an annular meridional cut with the colatitude $\theta \in [0, \pi]$ and the radius (in dimensionless units) $r \in [0.6, 1]$ i.e from slightly below the tachocline

($r = 0.7$) up to the solar surface, using the STELEM code. This code has been thoroughly tested and validated thanks to an international mean field dynamo benchmark involving 8 different codes (Jouve et al. 2008). At $\theta = 0$ and $\theta = \pi$ boundaries, both A_ϕ and B_ϕ are set to 0. Both A_ϕ and B_ϕ are set to 0 at $r = 0.6$. At the upper boundary, we smoothly match our solution to an external potential field, i.e. we have vacuum for $r \geq 1$. As initial conditions we are setting a confined dipolar field configuration, i.e. the poloidal field is set to $\sin \theta / r^2$ in the convective zone and to 0 below the tachocline whereas the toroidal field is set to 0 everywhere.

3.2. The standard physical ingredients and the modified surface source term

We now need to prescribe the amplitude and profile of the various ingredients acting in Eqs. (2) and (3), namely the rotation, the diffusivity, the meridional flow and the Babcock-Leighton source term.

The rotation profile captures some realistic aspects of the Sun's angular velocity, deduced from helioseismic inversions (Thompson et al. 2003), assuming a solid rotation below 0.66 and a differential rotation above the interface.

$$\Omega(r, \theta) = \Omega_c + \frac{1}{2} \left[1 + \operatorname{erf} \left(2 \frac{r - r_c}{d_1} \right) \right] (\Omega_{\text{Eq}} + a_2 \cos^2 \theta + a_4 \cos^4 \theta - \Omega_c), \quad (4)$$

with $\Omega_{\text{Eq}} = 1$, $\Omega_c = 0.93944$, $r_c = 0.7$, $d_1 = 0.05$, $a_2 = -0.136076$ and $a_4 = -0.145713$ and where erf is the error function. With this profile, the radial shear is maximal at the tachocline.

We assume that the diffusivity in the envelope η is dominated by its turbulent contribution whereas in the stable interior $\eta_c \ll \eta_t$. We smoothly match the two different constant values with an error function which enables us to quickly and continuously transit from η_c to η_t i.e.

$$\eta(r) = \eta_c + \frac{1}{2} (\eta_t - \eta_c) \left[1 + \operatorname{erf} \left(\frac{r - r_c}{d} \right) \right], \quad (5)$$

with $\eta_c = 10^9 \text{ cm}^2 \text{ s}^{-1}$ and $d = 0.03$.

In Babcock-Leighton flux-transport dynamo models, meridional circulation is used to link the two sources of the magnetic field namely the base of the CZ and the solar surface. For all the models presented in this paper we use a large single cell per hemisphere, directed poleward at the surface, vanishing at the bottom boundary $r = 0.6$ and thus penetrating a little below the tachocline. We take a stream function

$$\psi(r, \theta) = -\frac{2(r - r_b)^2}{\pi(1 - r_b)} \sin \left(\pi \frac{r - r_b}{1 - r_b} \right) \cos \theta \sin \theta, \quad (6)$$

which gives, through the relation $\mathbf{u}_p = \nabla \times (\psi \hat{e}_\phi)$, the following components of the meridional flow

$$u_r = -\frac{2(1 - r_b)(r - r_b)^2}{\pi r (1 - r_b)^2} \sin \left(\pi \frac{r - r_b}{1 - r_b} \right) (3 \cos^2 \theta - 1), \quad (7)$$

$$u_\theta = \left[\frac{3r - r_b}{1 - r_b} \sin \left(\pi \frac{r - r_b}{1 - r_b} \right) + \frac{r\pi}{1 - r_b} \frac{(r - r_b)}{(1 - r_b)} \cos \left(\pi \frac{r - r_b}{1 - r_b} \right) \right] \times \frac{2(1 - r_b)(r - r_b)}{\pi r (1 - r_b)} \cos \theta \sin \theta, \quad (8)$$

with $r_b = 0.6$.

In Babcock-Leighton dynamo models, the poloidal field owes its origin to the tilt of magnetic loops emerging at the solar surface. Since these emerging loops are thought to rise from the base of the convection zone through magnetic buoyancy, we see that we can directly relate the way we model the Babcock-Leighton (BL) source term and the results of 3D calculations shown in Sect. 2.

In the standard model, the source term is confined in a thin layer at the surface and is made to be antisymmetric with respect to the equator, due to the sign of the Coriolis force which changes from one hemisphere to the other. These features are retained in our modified version.

However, the standard term is proportional to the toroidal field at the base of the convection zone at the same time, implying an instantaneous rise of the flux tubes from the base to the surface where they create tilted active regions. The 3D calculations showed that the rise velocity and thus the rise time depend on the field strength at the base of the CZ, we thus introduce in our modified version of the source term, a magnetic field-dependent time delay in the toroidal field at the base of the convection zone. We thus take into account the time delay between the formation of strong toroidal structures at the base of the convection zone and the surface regeneration of poloidal field.

The modified expression of the source term is thus

$$S(r, \theta, B_\phi) = \frac{1}{2} \left[1 + \operatorname{erf} \left(\frac{r - r_2}{d_2} \right) \right] \left[\left| 1 - \operatorname{erf} \left(\frac{r - 1}{d_2} \right) \right| \right] \times \left[1 + \left(\frac{B_\phi(r_c, \theta, t - \tau_B)}{B_0} \right)^2 \right]^{-1} \times \cos \theta \sin \theta B_\phi(r_c, \theta, t - \tau_B), \quad (9)$$

where $r_2 = 0.95$, $d_2 = 0.01$, $B_0 = 10^4 \text{ G}$, with the time delay τ_B proportional to the inverse of the magnetic energy at the base of the convection zone, namely

$$\tau_B(\theta, t) = \tau_0 / B_\phi(r_c, \theta, t)^2.$$

In our 3D simulations, the approximate rise time for a $6 \times 10^5 \text{ G}$ field is indeed about 4 times that of a $3 \times 10^5 \text{ G}$ field. This takes into account the more significant effects of convective downdrafts and Ohmic diffusion in the “weak B” case. Note that the time delay is then dependent both on space and time.

Finally, we take into account the fact that very strong toroidal structures (more than 10^5 G) are not influenced by the Coriolis force enough to gain a significant tilt as they reach the surface. To do so, we introduce a quenching term in the surface source which will make the regeneration of the poloidal field less effective when the toroidal field at the base of the CZ is strong enough. Inversely, when the flux tubes are too weak, they will not be able to reach the surface at all, and will not take part into the regeneration term for the poloidal field. We thus prevent the weakest flux tubes (or equivalently the most delayed ones) to take part in the regeneration of poloidal fields at the surface. To do so, the source term is set to zero when the delays are above a certain threshold value corresponding to a rise time of approximately half a solar cycle.

4. Results

4.1. The standard solution

We first quickly present the solutions of our dynamo equations for the standard case which has been extensively discussed and

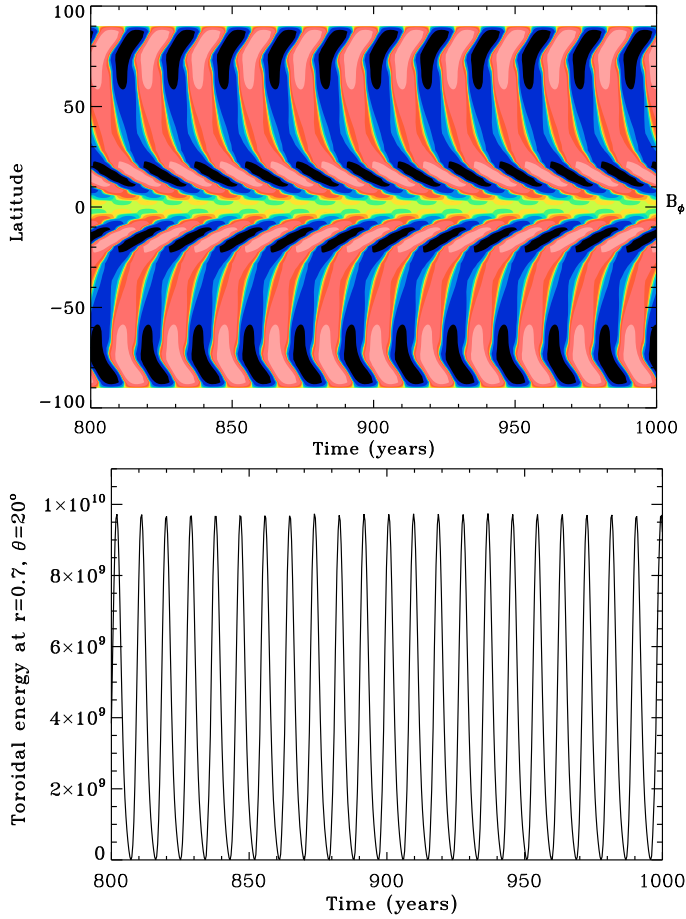


Fig. 2. Time-latitude cut of the toroidal field at the base of the convection zone (representing the butterfly diagram) and temporal evolution of the toroidal field energy (B_ϕ^2) at a particular position in space (at the base of the convection zone and at 20° in latitude in the Northern hemisphere). Time is in years and the magnetic field in Gauss. Red (blue) colours indicate positive (negative) field values, ranging from -2×10^5 G to 2×10^5 G.

used in the community to model the solar cycle (e.g. Dikpati & Charbonneau 1999).

Figure 2 shows the typical solution of a Babcock-Leighton standard dynamo model with a realistic choice of parameters. This is the same case as the reference case of Jouve & Brun (2007a). In particular, the maximum latitudinal velocity at the base of the convection zone (which is the significant velocity for the advection of strong toroidal fields close to the tachocline) is set to about $1 \text{ m}\cdot\text{s}^{-1}$.

The butterfly diagram resulting from this particular model is in good agreement with the observed migration of sunspots at the surface. In particular, a strong equatorward branch stretching from the mid-latitudes to the equator is clearly visible on the upper panel of Fig. 2. A strong poleward branch also appears in the evolution of the toroidal field at the interface, which is quite typical of Babcock-Leighton models. Indeed, it is the result of the combined action of low diffusivity at the base of the convection zone and strong radial shear linked to the differential rotation profile. It has been shown that both higher diffusivities (Dikpati & Charbonneau 1999) and penetration of the meridional flow below the core-envelope interface (Nandy & Choudhuri 2002) could prevent such a branch to appear. However, since our goal is more to study the effects of time delays in BL models than to

build a calibrated solar-like solution, we adopt this solution as our reference case.

Nevertheless, it has here to be pointed out that making the link between the evolution of toroidal field at the base of the convection zone and the sunspots location at the solar surface during a magnetic cycle is not straightforward. Indeed, to be able to make this link, we have to assume that the rise of toroidal structures from the base of the convection zone to the surface is radial. However, as Choudhuri & Gilman (1987) first demonstrated using the thin flux tube approximation and as Fan (2008) confirmed with 3D MHD simulations, initially weak magnetic flux tubes are deviated from the radial trajectory and tend to follow a path which is parallel to the rotation axis while they make their way to the solar surface. In the simulations presented here, we do not take into account this drift in latitude of weak structures but intend to do so in a future work. We thus assume the evolution of toroidal field at the base of the convection zone to be a good proxy for the sunspot migration at the surface but keep in mind that the butterfly diagram may take a different form if the latitudinal drift is taken into account.

The lower panel of Fig. 2 shows the time evolution of the toroidal field energy at the base of the convection zone and at the latitude of 20° , inside the activity belt. We clearly note that for the choice of parameters we made, the solution is harmonic in time, no modulation of the cycle is visible. As pointed out in the introduction, Charbonneau et al. (2005) showed that a variation of the strength of the Babcock-Leighton poloidal source term could lead to a chaotic behaviour of the solutions through a sequence of bifurcations. In order to focus on the influence of the time delays on the modulation of the cycle, we chose here a value of C_s which lies in the range of values for which no modulation of the cycle can arise for the standard solution.

4.2. Introducing moderate delays

We now turn to investigate the effect of introducing a magnetic field-dependent delay in the model, modifying the surface source term according to Eq. (9). In particular, we focus on the modification of the butterfly diagram and the evolution of the toroidal field energy at a particular point in space.

Figure 3 shows the butterfly diagram and toroidal field energy for a few cycles in the case where a small delay is introduced. More precisely, a delay of 14 days is imposed on 1 kG fields at the base of the convection zone. According to the dependence of the delay on the magnetic field intensity, it means that 10 kG fields will only be delayed by less than 4 hours, which is extremely small compared to the time scale of the magnetic cycle. However, even if the effects are hardly visible on the butterfly diagram (it is almost indistinguishable from the one of Fig. 2), a clear modulation of the magnetic energy appears on the lower panel of Fig. 3. The small modification of the butterfly diagram is not surprising considering the fact that the same physical processes still act in our model to generate and advect the 3 components of the magnetic field. In particular, the meridional flow, responsible for the advection of toroidal fields at the base of the convection zone, still acts to produce the characteristic equatorward branch of sunspot migration. What is more striking is the effect on the cycle amplitude which becomes modulated, while the cycle period remains approximately constant and identical to the standard case. To understand this particular feature, we will proceed to the study of a reduced model in the following section. But first, the effects of higher delays are analysed.

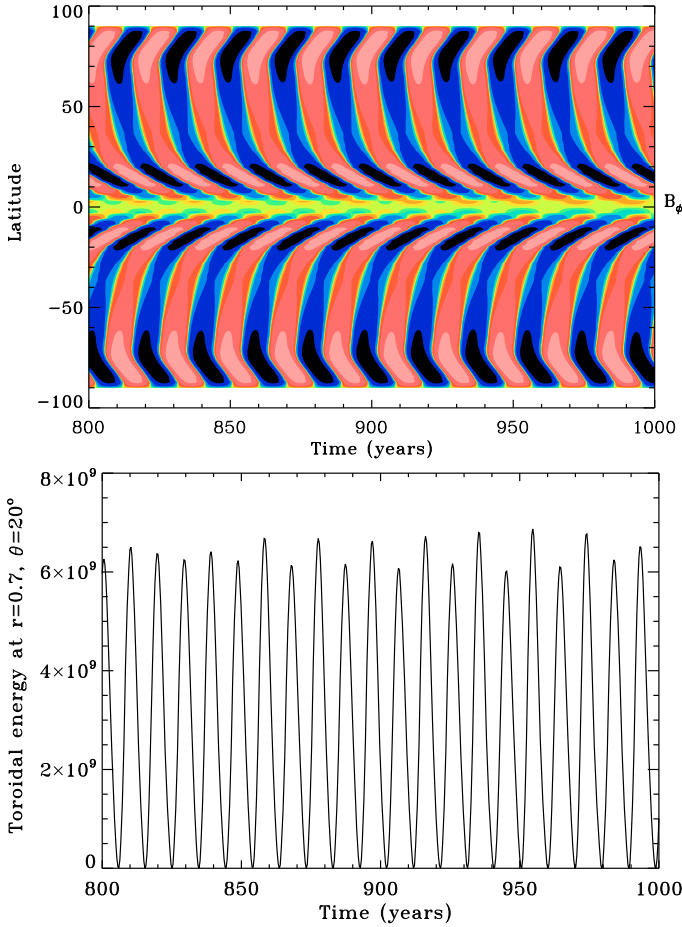


Fig. 3. Same as Fig. 2 but with a delay of 14 days on 1 kG fields.

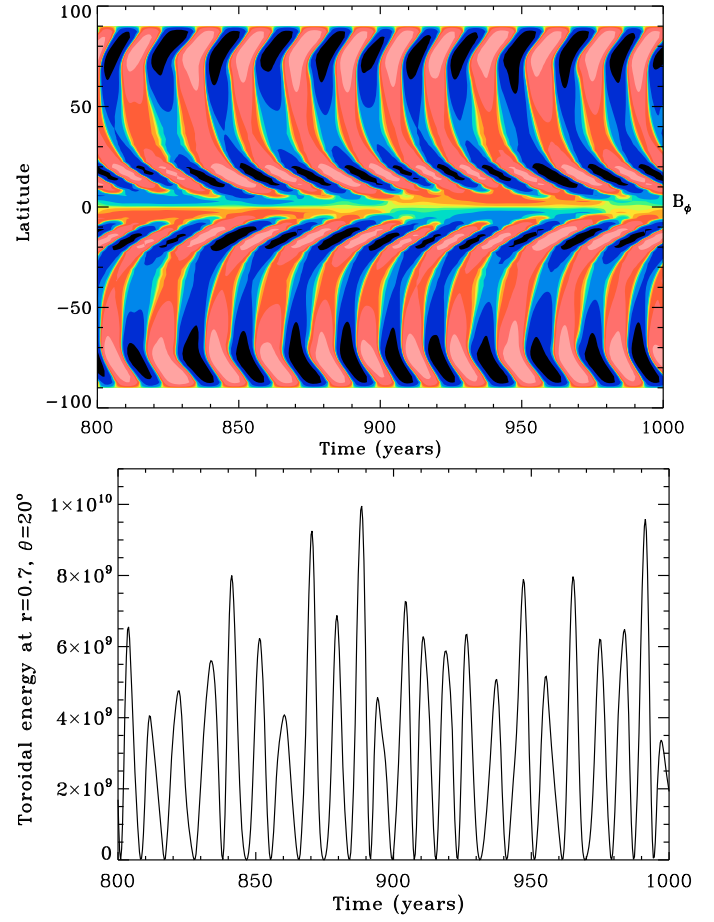


Fig. 4. Same as Fig. 2 but with a delay of 14 days on 50 kG fields.

4.3. Strong delays leading to highly perturbed solutions

The time delay is now increased from 14 days on 1 kG fields to 14 days on 50 kG fields, meaning that 10 kG fields will be delayed by almost a year in this case (compared to a few hours in the previous calculation). We point out again that the maximum delay which can be reached for very weak tubes is about 6 years (approximately half a cycle), since a longer time for toroidal structures to cross the convection zone would be unrealistic.

Figure 4 shows the butterfly diagram and the evolution of the magnetic energy for this case. This case is particularly interesting when we turn to consider the evolution of the toroidal energy with time. Indeed, again the effects on the shape of the butterfly diagram stay weak, even if some perturbations are clearly visible. In particular, close to the equator, consecutive cycles of the same polarity seem to connect, leading the cycle period at these latitudes to be different from the basic 11-yr cycle still present at higher latitudes. We also note that the period varies from one cycle to another but this particular feature is even more visible on the lower panel of Fig. 4.

The major effect of the delays is again to modulate the amplitude of the cycle to such a point that the weakest cycle on the particular period shown in Fig. 4 reaches in terms of peak energy only 30% of the peak energy of the strongest cycle. These variations are comparable to the observations of the monthly sunspot number available from 1750 until today (e.g. Hoyt & Schatten 1998). Indeed, over this period of time, the weakest cycle (cycle 5, which reached its peak in 1804) has been shown to possess a sunspot number of about 50 whereas the strongest cycle

(cycle 19, which reached its maximum value in 1955) reached a sunspot number of more than 200. These strong variations are thus reproduced in this model with rather strong delays, but still small compared to the cycle period.

Finally, we should stress the variety of morphologies exhibited by the different cycles. In particular, some cycles show a clear asymmetry between their rising and declining phases (for example the cycle peaking at $t = 895$). Interestingly, we also note that some cycles seem to possess almost two peaks (as was observed on cycle 23) or at least show a change of slope in the declining phase, which makes them quite different from the standard more “classical” cycle.

To better understand the results of such a modulation in the amplitude and possibly on the period of the modelled solar cycle, we need to get back to a reduced model and analyse its properties from a dynamical systems point of view.

5. Understanding the modulation: reduction to a 6th order system

5.1. Formulation and justification of the reduced model

The reduced model we decide to use does not explicitly contain time-delays as in the 2D model. It rather introduces another variable Q which will be delayed by time τ with respect to the toroidal field B . Moreover, we now work in only one dimension

in space. The set of equations we thus want to solve here is the following:

$$\frac{\partial A}{\partial t} + v \frac{\partial A}{\partial x} = \frac{SQ}{1 + \lambda|Q|^2} + \eta \frac{\partial^2 A}{\partial x^2}, \quad (10)$$

$$\frac{\partial B}{\partial t} + v \frac{\partial B}{\partial x} = \Omega \frac{\partial A}{\partial x} + \eta \frac{\partial^2 B}{\partial x^2}, \quad (11)$$

$$\frac{\partial Q}{\partial t} = \frac{1}{\tau} (B - Q). \quad (12)$$

This model is significantly simplified since the physical ingredients (the rotation rate, the magnetic diffusivity, the meridional flow and the source term) are taken to be constants. τ is still dependent on the inverse of the toroidal field B , leading to the following expression:

$$\tau = \frac{\tau_0}{1 + |B|^2}.$$

We will nevertheless show that such a simple model with a varying time delay, even small, is able to reproduce a modulation in the cyclic behaviour of the solutions.

In order to simplify even more the previous set of equations, we take the variables A , B and Q to be single Fourier modes in x , with wavenumber k , such that:

$$A(x, t) = A_t(t) \exp(ikx),$$

$$B(x, t) = B_t(t) \exp(ikx),$$

$$Q(x, t) = Q_t(t) \exp(ikx),$$

we then get the following set of complex ODEs:

$$\frac{dA_t}{dt} + ikvA_t = \frac{SQ_t}{1 + \lambda|Q_t|^2} - \eta k^2 A_t, \quad (13)$$

$$\frac{dB_t}{dt} + ikvB_t = ik\Omega A_t - \eta k^2 B_t, \quad (14)$$

$$\frac{dQ_t}{dt} = \frac{1}{\tau} (B_t - Q_t), \quad (15)$$

with $\tau = \tau_0 / (1 + |B_t|^2)$. All the analysis of the previous set of ODEs will be made considering $k = 1$ to be the wavenumber of interest in our model. This system possesses 6 degrees of freedom represented by the real and imaginary parts of each variables A_t , B_t and Q_t .

This choice of model was motivated by the fact that we want to study this set of ODEs as a dynamical system. Having explicit delays in the equations makes it much more difficult to identify the sequence of bifurcations which could occur between the harmonic solution of Fig. 2 and the aperiodic solution of Fig. 4. Nevertheless, the new variable Q_t introduced in our simplified model and which now represents the delayed toroidal field behaves exactly as we want it to. To illustrate this, we solve the set of equations numerically for the following choice of parameters: $\Omega = 100$, $S = 100$, $\eta = 10^{-3}$, $v = 10^{-2}$, $\lambda = 10^{-4}$ and $\tau_0 = 2 \times 10^{-2} B_1^2$ where $B_1 = 3 \times 10^8$ is a normalization factor. From now on, the values of τ_0 will be expressed in terms of multiples of B_1^2 . We note here that the actual time delays should not be directly related to the values of τ_0 , because of this normalization factor.

These parameters are difficult to relate to the ones used in the full 2D model but they were chosen so that:

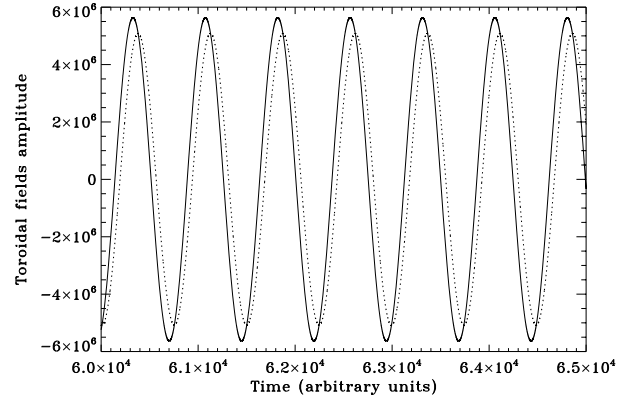


Fig. 5. Temporal evolution of the toroidal field (plain line) and delayed toroidal field (dotted line) for a case where the delay is small enough to keep the harmonic solution stable.

- dynamo action occurs (the dynamo number is high enough);
- the standard solution is harmonic in time (the dynamo number is low enough so it does not lead to any modulation of the cycle);
- we lie in the advection-dominated regime rather than in the diffusion-dominated one (the advection time $1/kv$ is shorter than the diffusive time $1/k^2\eta$, leading to $v > \eta$ in our case where $k = 1$);
- the time delay is always smaller than half a cycle period (i.e. we impose a maximum value for the time delay, like we did in the 2D model where the source was set to zero when the delay was too long).

Figure 5 shows the evolution over a few cycles of the toroidal field $\Re(B_t)$ and the delayed toroidal field $\Re(Q_t)$. We can notice two major particularities: first, we clearly note the time shift between the two fields, representing the time delay imposed by the value of τ_0 . In this case, the solution is harmonic and hence $|B_t|^2$ is constant and thus the time delay is also constant. Consequently, the time shift between the two fields is always the same along the different cycles which are represented on the figure.

The second point which has to be noticed is the significantly lower amplitude of $\Re(Q_t)$ compared to the original toroidal field $\Re(B_t)$. This amplitude difference is due to the fact that the evolution equation for Q_t is similar to a diffusion equation. This property models the ohmic diffusion acting on the toroidal flux tubes during their rise through the convection zone. Indeed, we can reasonably expect the flux tubes reaching the surface to have a lower amplitude than at the base of the convection zone. Moreover, the decrease in strength will be higher when the initial magnetic field intensity in the flux tubes is lower. Indeed, when the flux tubes are weaker, their rise time is longer and becomes comparable to the diffusive time associated to the magnetic structure, which is equal to a^2/η when the rising flux tube has a circular section of radius a . In our reduced model, this effect is also taken into account since the time delay for weaker tubes will be higher and thus the diffusion operator will be more efficient in this case.

With this choice of model and parameters, we are thus close to the dynamo solution calculated with the STELEM code presented in the previous section, so that we can reasonably relate the results of the reduced model to the full 2D calculations. The major interest of this type of models is that we are now reduced to a 6th order system which can be analysed both analytically and numerically.

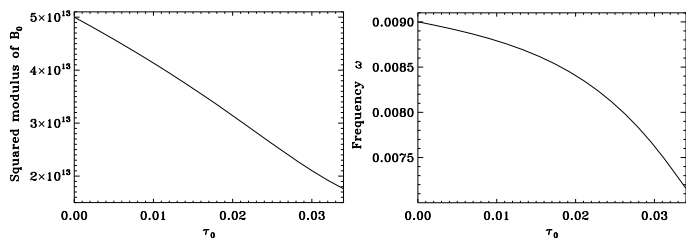


Fig. 6. Variation of the amplitude and the frequency of the toroidal field B_t with the delay, for a particular case. The choice of parameters is the same as in the previous section, namely: $\Omega = 100$, $S = 100$, $\eta = 10^{-3}$, $v = 10^{-2}$, $\lambda = 10^{-4}$.

5.2. Destabilization of the harmonic solution and influence of parameters

We now proceed to the analytic study of the characteristics of the harmonic solution when the delay is increased. In particular, we investigate the influence of the model parameters on the amplitude and frequency of the harmonic solution. The details of this analysis are presented in Appendix A.

As expected, the dynamo number $\Omega S/\eta$ controls the amplitude of our solution while the meridional flow speed sets the cycle period. This behaviour is characteristic of mean-field flux transport dynamo model and we are thus not going into too many details. The effects of an increasing delay on both the frequency and the amplitude of the solution is on the contrary of some interest for our particular study.

Figure 6 shows the variation of the amplitude and frequency of the harmonic solution when the delay is increased when all the other parameters are fixed to the values quoted in the previous section. For higher values of the delay, the solution becomes unstable, as we will see in the stability analysis below. The standard “undelayed” solution is also included in these plots, for $\tau = \tau_0 = 0$. We note that the amplitude of our solution decreases linearly with the delay which can be explained by the fact that the amplitude of $\Re(Q_t)$ (which represents the delayed toroidal field and thus is the one responsible for the regeneration of the poloidal field A_t) is smaller than the amplitude of B_t , due to the diffusive effects included in our equations. Hence, the amount of poloidal field generated by the reduced toroidal field will be weaker and consequently, the toroidal field produced through the Ω -effect acting on the poloidal field will also be reduced.

The frequency of the solution has a different behaviour when τ is increased. Indeed, the variation is first close to linear with τ , meaning that the cycle period is increased linearly with the delay but then the slope of the curve changes and the cycle is significantly slowed down by a variation of the delay. This feature can also be understood by the fact that the regeneration of poloidal field will take longer and longer when the delay is increased and thus the dynamo loop will take longer to close.

Another interesting point here is that we can study the effect of the various parameters on the threshold above which the harmonic solution becomes unstable. We will not focus on the effect of the dynamo number on this threshold since it has been studied in similar conditions before. Instead, we fix the dynamo number and we investigate the evolution of this threshold when the meridional flow speed is increased. The detailed stability analysis is shown in Appendix B. It has to be pointed out here that a Floquet analysis has been applied to our equations to investigate the nature of the bifurcation undergone by the system at that threshold. We find that two imaginary conjugate Floquet multipliers (reflecting the behaviour of a perturbation to the periodic

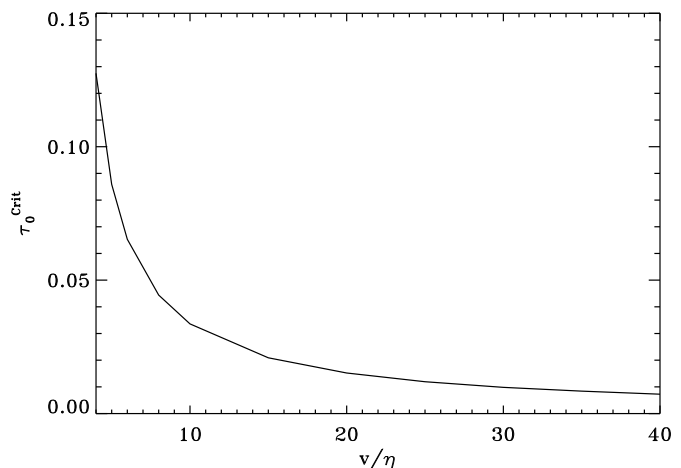


Fig. 7. Value of τ_0 for which the harmonic solution becomes unstable with respect to the normalized meridional flow speed.

solution after one cycle) cross the unit circle, thus indicating a Hopf bifurcation.

Figure 7 shows the dependence of the critical τ_0 (i.e. the value for which the harmonic solution becomes unstable) with the meridional flow speed normalized by the magnetic diffusivity. In our particular case where $k = 1$ (and thus where v/η represents the ratio between diffusive and advective times), this gives us some insight on the value of the delay which has to be reached to get a modulation, when the system tends more and more towards an advection dominated regime. The trend of the threshold to decrease with increasing meridional flow speed is not surprising if we consider we are introducing fixed values for the delays, not normalized to the cycle period. Indeed, as v is increased, the cycle period is decreased and then the absolute value for the delay to have a significant effect on the cycle is decreased. What is more striking is the saturation that the curve seems to reach when v is increased to strong values. In this case, the cycle period (which is roughly inversely proportional to the meridional flow speed in this type of models) is still decreased but the critical value for the delay seems to reach a minimum value. We thus conclude that the percentage of the cycle represented by the critical delay will increase when the meridional flow speed is increased. As an example, in the case where the meridional flow speed is quite weak ($v/\eta = 4$), the threshold delay represents about 14% of the cycle period whereas at $v/\eta = 40$, this percentage reaches 30%. In this strongly advection-dominated regime, the meridional flow speed is probably dominating the time-scale of the system and as a result the effect of the delays is reduced.

In the remainder of the paper, we focus on an intermediate case ($v/\eta = 10$), where the threshold value for the delay ($\tau_0 \approx 3.36 \times 10^{-2}$) reaches 19% of the cycle. This value can appear quite large to the typical values for the delay used in the full 2D model but it has to be pointed out that as soon as the modulation appears, the strongest fields reach higher values than the peak values of the harmonic solution. As a consequence, the delays for the strongest fields are shorter and reach about 8% of the cycle, which is closer to what was used in the 2D model. This remark is related to the effect of fixed versus varying delays, which we discuss in the conclusion.

5.3. Further evolution

Knowing the behaviour of the harmonic solution (which is stable for small values of the delay) and the influence of the parameters,

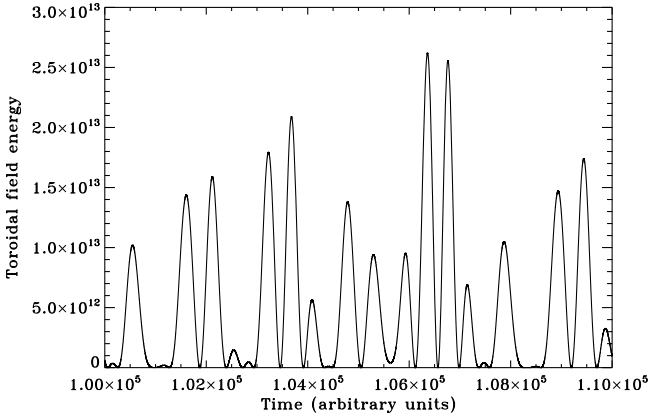


Fig. 8. Time evolution of the toroidal magnetic energy with a value of the delay of $\tau_0 = 9 \times 10^{-2}$. Aperiodic modulation of the cyclic pattern is now fully developed.

we choose a particular set of those parameters to try to study a generic solution when the delay is further increased. We thus choose numbers which satisfy the conditions invoked in Sect. 5.1 and a meridional flow speed in agreement with what was shown in the previous section. The parameters chosen for all the analysis are the following: $\Omega = 100$, $S = 100$, $\eta = 10^{-3}$, $v = 10^{-2}$, $\lambda = 10^{-4}$, the same as the ones used for the solution shown in Fig. 6.

Figure 8 shows the time series of the toroidal magnetic energy for the solutions of the system when the delay is further increased to $\tau_0 \approx 9 \times 10^{-2}$. An aperiodic modulation of the solar cycle is here clearly visible, and the major point is that the evolution of toroidal energy is very similar to what was found in the full 2D system when the delay was sufficiently large (see Fig. 4). Indeed, the major modulation acts on the cycle amplitude but the frequency also varies and periods of very low activity arise. This type of behaviour is very attractive when compared to the observed sunspot number which qualitatively shows the same kind of long-term variations. We should stress that we are still here in a regime where the time delays are small compared to the long-term modulation they seem to create. Moreover, this perturbed solution is obtained both through 2D mean-field simulations and through a reduced set of ODEs solving the Babcock-Leighton dynamo problem. These results are thus of particular interest as a new origin of modulation seems to appear: the time delays due to the buoyant rise of flux tubes from the base of the convection zone to the solar surface to create active regions. We now need to understand what happens to the system between the first bifurcation and this aperiodic more interesting solution.

We thus turn to investigate in more details which sequence of bifurcations leads to such complicated behaviour.

6. Beyond the first bifurcation: reduction to a 5th order system

To gain some insight on the behaviour of the system after the first bifurcation, we show that we can further reduce our problem from a 6th order to a 5th order system. Indeed, it is rather impractical to study the precise behaviour of the system after the first bifurcation. Reducing our system even more will help us achieve this goal.

6.1. Formulation of the model

Noticing that our system possesses a phase-invariance, i.e. a further symmetry, we follow the procedure of Weiss et al. (1984) and Jones et al. (1985) and make a change of variables which will remove this symmetry.

We express our variables A_t , B_t and Q_t using polar coordinates and introduce four new variables as shown

$$A_t = \rho y e^{i\theta},$$

$$B_t = \rho e^{i\theta},$$

$$Q_t = \rho z e^{i\theta},$$

where y and z are complex numbers and θ and ρ are real. The real numbers ρ and θ here represent respectively the modulus and argument of the basic toroidal field B_t . We can now reintroduce these expressions in Eqs. (13)–(15) to get, after some algebra, the new set of ODEs

$$\dot{\rho} = -\Omega \rho \Im(y) - \eta \rho \quad (16)$$

$$\dot{y} = \frac{S z}{1 + \lambda \rho^2 |z|^2} - i \Omega y^2 \quad (17)$$

$$\dot{z} = \frac{1 - z}{\tau} - (i \Omega y - i v - \eta) z, \quad (18)$$

where

$$\tau = \frac{\tau_0}{1 + \rho^2}.$$

We then get a 5th order system since y and z are complex but ρ is real. We find that θ , which is the phase of the “undelayed” toroidal field, does not appear explicitly in this new set of equations but can be obtained from

$$\dot{\theta} = \Omega \rho \Re(y) - v \rho. \quad (19)$$

The interesting outcome of reducing our system from 6 degrees of freedom to 5 is that the limit cycle of the higher-order system now corresponds to a stationary solution in our reduced model and that a torus now corresponds to a limit cycle.

Solving this new system numerically will now enable us to analyze the further evolution of our solution when the delay is increased. In particular, we show that we can now easily exhibit the sequence of bifurcations leading to the aperiodic modulation of Fig. 8.

6.2. From the harmonic to the aperiodic solution: a sequence of bifurcations

We follow the evolution of our system from the first bifurcation at $\tau_0 = 3.36 \times 10^{-2}$ to the aperiodic solution at $\tau_0 = 9 \times 10^{-2}$. First, we can relate again these values to some physically meaningful time-delays, keeping in mind that the system has been simplified and that a particular choice of parameters was made. For the stronger fields, a value of $\tau_0 \approx 3.36 \times 10^{-2}$ would then correspond to a delay of approximately a tenth of the cycle duration and $\tau_0 \approx 9 \times 10^{-2}$ a third of the cycle period. These delays may look higher than what was calculated in the 2D model but we showed that a modification of the parameters (and especially of the meridional flow speed) could move the threshold above which the modulation starts to appear.

The Floquet multipliers for this system are computed in order to study the stability of our periodic solution. We find that

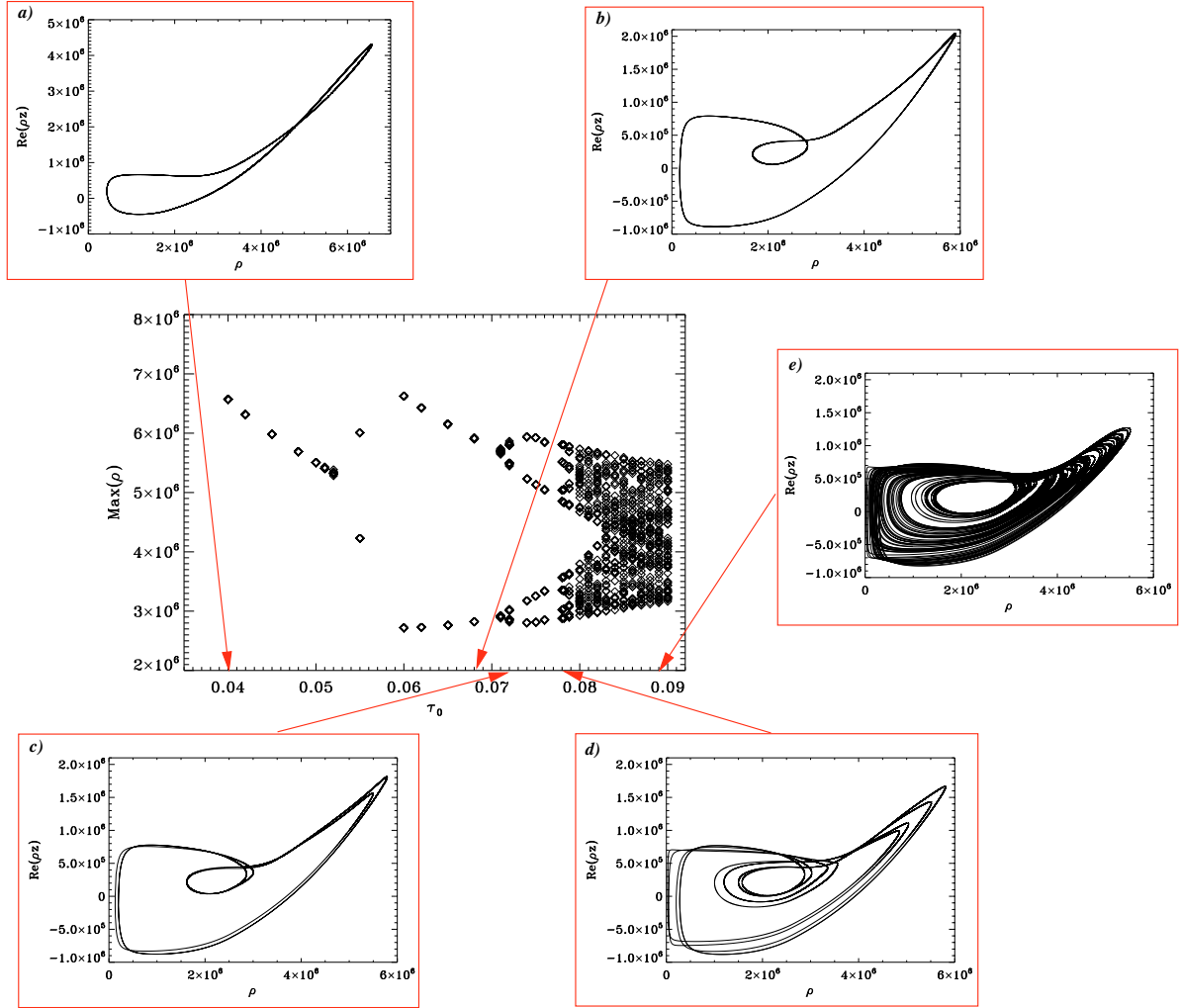


Fig. 9. Evolution of the system after $\tau_0 = 4 \times 10^{-2}$: bifurcation diagram and phase portraits in the $(\rho, \Re(\rho z))$ plane for values of the control parameter τ_0 close to those for which successive period doublings occur.

the solution of our new reduced model stays on a periodic orbit for a large range of values for the delay, i.e. from 3.36×10^{-2} to about 5.43×10^{-2} . We indeed find that at this value for the parameter τ_0 , one of the real Floquet multipliers crosses the unit circle through the -1 point, indicating a period doubling bifurcation. This new 2-periodic solution then persists for quite a large range of the control parameter until we reach a new period doubling bifurcation.

Figure 9 shows the evolution of the system from the periodic solution resulting from the first Hopf bifurcation at $\tau_0 \approx 3.36 \times 10^{-2}$ until we reach the aperiodic modulations of the cycle. We present on this figure a bifurcation diagram computed by determining the maximum values of ρ for each value of $\tau_0 \geq 4 \times 10^{-2}$ (when the first period doubling has already occurred). The initial branch existing at the beginning of the bifurcation diagram thus indicates a periodic orbit. Moreover, phase portraits at key values of the parameter are shown. They were chosen to stress the sequence of period doubling bifurcations exhibited by the set of ODEs. Panel b) shows the modification of the phase portrait of panel a) after the first period doubling has occurred. We are then in the presence of a 2-periodic solution: every 2 cycles, the value of ρ reaches the same maximum value and this behaviour persists for as long as the model has been calculated, i.e. for thousands of cycles. At $\tau_0 \approx 7.15 \times 10^{-2}$, the system goes through another bifurcation. The period is doubled

again, which is visible both on the bifurcation diagram (where the number of points is doubled at this value) and on panel c). Indeed, the curve on the phase portrait closes on itself after 4 cycles now instead of 2 for the previous values of τ_0 . Period doublings happen again at $\tau_0 \approx 7.8 \times 10^{-2}$ and $\tau_0 \approx 7.88 \times 10^{-2}$ where the solution becomes first 8-periodic and then 16-periodic. The phase portrait on panel d) shows the time needed to close the curve is doubled at $\tau_0 \approx 7.8 \times 10^{-2}$ compared to the solution of panel c). But obviously, since the curve is still closed, the system is still periodic.

It then becomes difficult to identify further period doublings but they may occur in very narrow windows for the parameter. The main point is that the system seems to reach a very complicated behaviour when the value of τ_0 approaches 8.5×10^{-2} . Panel e) shows the phase portrait for $\tau_0 = 8.8 \times 10^{-2}$. The phase space is almost entirely covered by the solution and any value can be reached by the peaks in the temporal evolution of ρ , as shown on the bifurcation diagram. At this stage, a clear periodicity is difficult to identify and we recover the strongly modulated solution shown in Fig. 8 for a value of the parameter of 9×10^{-2} .

Consequently, our system seems to undergo a sequence of period doublings leading to a chaotic behaviour. The solution may well be modified for higher values of the time-delays but which would not be realistic anymore for the physical process we are modelling. Similar cascades of period doublings

have been found in the Lorenz equations (Sparrow 1982) and in other systems of ordinary and partial differential equations, including those governing the solar dynamo (Moore et al. 1983; Knobloch & Weiss 1983; Weiss et al. 1984; Knobloch et al. 1998). However, the nonlinearities at the origin of the sequence of bifurcations in those models were always related to the dynamical feedback of the Lorentz force on the flow. The striking result in this work is that modulation of the cycle amplitude can also arise in models where the only nonlinearities are the quenching term in the Babcock-Leighton source and the magnetic field-dependent time delays. It has here to be noted though that the time delays also appear in the quenching term (see Eq. (9)), possibly amplifying the nonlinear effects in the model.

We conclude that time delays due to flux tubes rising from the base of the convection zone to the surface seem to create a strongly modulated cycle in Babcock-Leighton dynamo models. A sequence of period doublings leading to chaos has clearly been identified here thanks to our 5th-order system. Indeed, even though it is also obviously present in the 6th order system, it is much more difficult to exhibit. The magnetic cycle resulting from these models which take into account the rise time of toroidal fields thus seems to be closer to the actual behaviour of the solar cycle.

7. Discussion and conclusion

In this work, we have introduced a more physically accurate model for the poloidal field source term in Babcock-Leighton flux transport dynamo models. To do so, some results from 3D MHD calculations of rising flux tubes from the base of the convection zone to the surface were reintroduced in 2D mean-field models. In particular, the rise time of flux ropes, which was assumed to be negligible in previous simulations, was here taken into account by introducing magnetic energy-dependent time delays in the BL source term. Through the use of a combination of analytical and numerical techniques applied to an adapted reduced system of non linear equations, we show that the system exhibits a sequence of bifurcations leading to a chaotic behaviour. The time evolution of the solution at that stage is qualitatively very similar to the full 2D model and more importantly to the actual solar activity, with strong modulation especially on the cycle amplitude.

Assuming the rise of flux tubes from the base of the convection zone and the surface to be instantaneous and thus the time delays due to magnetic buoyancy to be negligible can sound reasonable since these delays are weak compared to the other time-scales of the system. In particular, we can expect the time delay due to the advection by the meridional flow (which has a characteristic time-scale of a few solar cycles, see for example Charbonneau & Dikpati 2000) to be much more effective on the behaviour of the dynamo-generated magnetic field. As a consequence, it is mainly the effect of meridional flow which has been tested in previous models (e.g. Wilmot-Smith et al. 2006). However, we showed here that the time delays due to flux tubes rising have in fact a significant effect to modulate the cycle on time scales very large compared to the delays. The main reason for this behaviour is that the delays are not fixed but depend on the modulated toroidal energy itself. To illustrate this explanation, we show in Fig. 10 the time evolution of toroidal fields (delayed and undelayed) for a case similar to what we showed in the core of the paper (a $|B|^2$ -dependent delay with $\tau_0 = 3.4 \times 10^{-2}$, i.e. just after the Hopf bifurcation) and the same evolution when the delay is fixed to the mean value reached by the delay in the previous run.

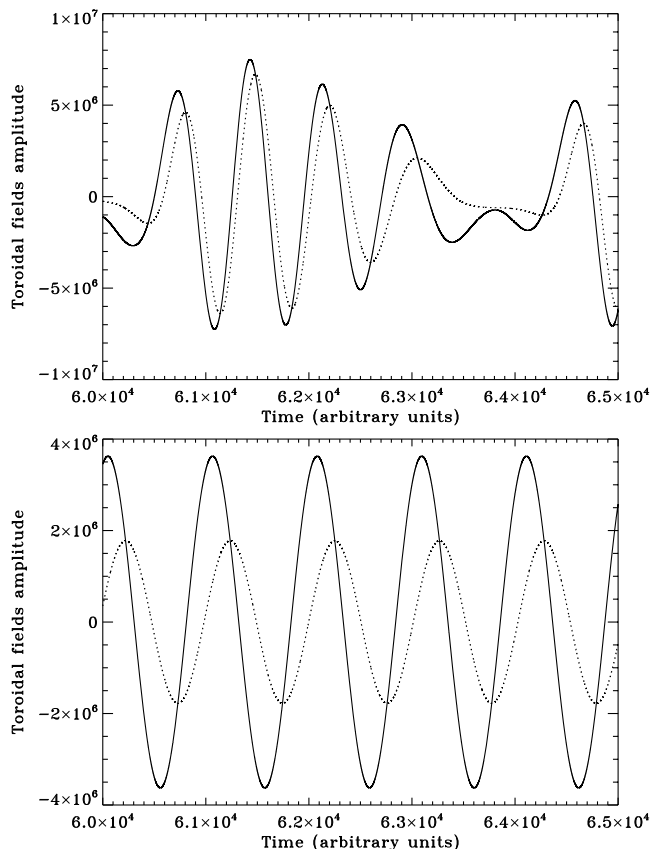


Fig. 10. Time evolution of the toroidal fields amplitude (undelayed in plain line and delayed in dotted line) for a delay dependent on $|B|^2$ just after the Hopf bifurcation (*upper panel*) and for a delay fixed to the mean value of the previous run (*lower panel*).

On this figure, both the basic toroidal field and the delayed field are shown, stressing the time shift existing between the two. The striking result is that a long-term modulation appears only in the case of a varying delay. In the fixed-delay case, although the time-shift between the basic toroidal field and its delayed counterpart is quite significant compared to the cycle period, no modulation is created. On the contrary, in the varying-delay case, even though the strongest fields are almost not affected by the time-shift, a strong modulation on the amplitude is built up. As a result, the fact that small delays can affect the long-term evolution of the dynamo cycle seems to be linked to the variability of these delays and more specifically to their dependence on the magnetic field strength. Since magnetic buoyancy is much more efficient in the solar interior for strong toroidal field structures, these delays are likely to appear in reality. Consequently, a new origin of the solar cycle modulation may have been revealed here, thanks to the input of 3D MHD models into 2D mean-field dynamo calculations.

Only a part of the results of 3D calculations were reintroduced here but other effects can also be taken into account. In particular, hoop stresses and the Coriolis force are known since the first thin flux tubes simulations to deflect the trajectory of buoyantly rising magnetic fields inside the convection zone, this effect being stronger when the fields are less intense. This feature could also be introduced in BL models by modifying the source term for poloidal field. In particular, the source term is likely to get a contribution from the same latitude as the initial position of the flux tubes when those are strong enough and from a lower latitude when the flux tubes have been sufficiently influenced by

the Coriolis force and the hoop stresses to rise parallel to the rotation axis. This may result in a different shape for the butterfly diagram with slightly more activity at higher latitudes, provided that weak magnetic structures are assumed to be able to reach the surface and create active regions. This could lead to reconsider the correspondence which is often made between toroidal magnetic field generated in 2D dynamo models at the base of the convection zone and the actual sunspot migration observed at the solar surface.

The variations of the solar cycle period are also known to be significant. For instance, cycle 23 has been significantly longer than the previous ones, with a duration of about 13 years (1996–2009). In the models computed in this work, the modulation of the solar activity is particularly visible on the cycle amplitude and is much less obvious on the period. However, the influence of rising flux tubes on the meridional flow was not taken into account here. Since the cycle period of the solutions resulting from these flux-transport models is very sensitive to the amplitude of the meridional circulation, a modification of the flow by rising flux tubes is very likely to modify the frequency of the dynamo solution and thus to also introduce a modulation on the cycle period. This feature is currently being investigated.

A considerable step forward would obviously be to develop a self-consistent global model with buoyant toroidal structures built up and making their way from the base of the convection zone where they become unstable to the photosphere where they create active regions. Unfortunately, this has not been achieved yet due to numerous physical and numerical difficulties. In the mean time, we have shown here that inputs from 3D MHD models simulating a particular step of the dynamo cycle can significantly improve 2D mean-field calculations. In particular, we have shown that they can even help reproducing a feature of the solar cycle (its variability) which was not present in the standard model before. We will continue to develop these ideas in future work.

Acknowledgements. L.J. and G.L. acknowledge support by STFC.

Appendix A: Amplitude and frequency of the harmonic solution

We can further expand our harmonic solution on a single Fourier mode in time as:

$$A_t(t) = A_0 \exp(i\omega t),$$

$$B_t(t) = B_0 \exp(i\omega t),$$

$$Q_t(t) = Q_0 \exp(i\omega t).$$

Reintroducing these expansions in Eqs. (13)–(15) will give us a way to calculate the frequency ω and the amplitude of the harmonic solution $|B_0|$ or equivalently $|Q_0|$ with respect to all the parameters. The complex dispersion relation we get with $k = 1$ is the following

$$(i\omega + i\nu + \eta)^2 (i\omega\tau + 1) = \frac{i\Omega S}{1 + \lambda|Q_0|^2}. \quad (\text{A.1})$$

Taking the real and imaginary parts of this relation dispersion give us the following equations

$$\omega^2(1 + 2\eta\tau) + 2\omega\nu(1 + \tau\eta) + \nu^2 - \eta^2 = 0 \quad (\text{A.2})$$

$$\omega^3\tau + 2\omega^2\nu\tau + \omega(\nu^2\tau - \eta^2\tau - 2\eta) = -\frac{\Omega S}{1 + \lambda|Q_0|^2} + 2\eta\nu \quad (\text{A.3})$$

where

$$\tau = \tau_0/(1 + |B_0|^2).$$

Appendix B: Stability of the harmonic solution

We can focus on the stability of this periodic solution by perturbing it and studying the growth rates of the perturbations. To do so, we perturb the solution as follows

$$\tilde{A} = A_t (1 + \alpha_1 e^{pt} + \alpha_2^* e^{p^*t}) \quad (\text{B.1})$$

$$\tilde{B} = B_t (1 + \beta_1 e^{pt} + \beta_2^* e^{p^*t}) \quad (\text{B.2})$$

$$\tilde{Q} = Q_t (1 + \gamma_1 e^{pt} + \gamma_2^* e^{p^*t}) \quad (\text{B.3})$$

where $\alpha_1, \alpha_2, \beta_1, \beta_2, \gamma_1$ and γ_2 represent the coefficients of the perturbed fields, p represents the complex growth rate of the perturbation and the symbol \star stands for the complex conjugate.

Substituting these expressions in Eqs. (13)–(15) give us a system of 6 equations relating the coefficients of the perturbations, the growth rate and all the parameters of the system.

$$(i\omega + p + \eta + i\nu)\alpha_1 = (i\omega + \eta + i\nu) \left[\gamma_1 - \frac{\lambda|Q_0|^2}{1 + \lambda|Q_0|^2} (\gamma_1 + \gamma_2) \right]$$

$$(-i\omega + p + \eta - i\nu)\alpha_2 = -(i\omega - \eta + i\nu) \left[\gamma_2 - \frac{\lambda|Q_0|^2}{1 + \lambda|Q_0|^2} (\gamma_1 + \gamma_2) \right]$$

$$(i\omega + p + \eta + i\nu)\beta_1 = (i\omega + \eta + i\nu)\alpha_1$$

$$(-i\omega + p + \eta - i\nu)\beta_2 = (-i\omega + \eta - i\nu)\alpha_2$$

$$\left(i\omega + p + \frac{1 + |B_0|^2}{\tau_0} \right) \gamma_1 =$$

$$\left(i\omega + \frac{1 + |B_0|^2}{\tau_0} + \frac{i\omega|B_0|^2}{1 + |B_0|^2} \right) \beta_1 + \frac{i\omega|B_0|^2}{1 + |B_0|^2} \beta_2$$

$$\left(i\omega - p - \frac{1 + |B_0|^2}{\tau_0} \right) \gamma_2 =$$

$$\left(i\omega - \frac{1 + |B_0|^2}{\tau_0} + \frac{i\omega|B_0|^2}{1 + |B_0|^2} \right) \beta_2 + \frac{i\omega|B_0|^2}{1 + |B_0|^2} \beta_1$$

$|B_0|^2$ and $|Q_0|^2$ being related by the following expression

$$|Q_0|^2 = \frac{|B_0|^2(1 + |B_0|^2)^2}{\omega^2\tau_0^2 + (1 + |B_0|^2)^2}.$$

A non-trivial solution for this system exists only if the determinant is zero, we thus have to calculate the determinant and find the roots of the 6th order polynomial, in terms of the growth rate p . The harmonic solution loses stability at a Hopf bifurcation when the real part of one of the roots becomes positive.

References

- Archontis, V., Moreno-Insertis, F., Galsgaard, K., & Hood, A. W. 2005, *ApJ*, 635, 1299
- Babcock, H. W. 1961, *ApJ*, 133, 572
- Bard, E., & Frank, M. 2006, *Earth Planet. Sci. Lett.*, 248, 1
- Brun, A. S., Miesch, S. M., & Toomre, J. 2004, *ApJ*, 614, 1073
- Bushby, P. J. 2006, *MNRAS*, 371, 772
- Caligari, P., Moreno-Insertis, F., & Schüssler, M. 1995, *ApJ*, 441, 886
- Cattaneo, F. 1999, *ApJ*, 515, L39
- Cattaneo, F., Brummell, N. H., & Cline, K. S. 2006, *MNRAS*, 365, 727
- Charbonneau, P. 2005, *Liv. Rev. Sol. Phys.*, 2
- Charbonneau, P., & Dikpati, M. 2000, *ApJ*, 543, 1027
- Charbonneau, P., St-Jean, C., & Zacharias, P. 2005, *ApJ*, 619, 613
- Cheung, M. C. M., Schüssler, M., & Moreno-Insertis, F. 2007, *A&A*, 467, 703

- Choudhuri, A., & Gilman, P. 1987, *ApJ*, 316, 788
- Cline, K. S. 2003, Ph.D. Thesis
- Clune, T. L., Elliott, J. R., Glatzmaier, G. A., Miesch, M. S., & Toomre, J. 1999, *Parallel Comput.*, 25, 361
- D'Silva, S., & Choudhuri, A. R. 1993, *A&A*, 272, 621
- Dikpati, M., & Charbonneau, P. 1999, *ApJ*, 518, 508
- Dikpati, M., & Gilman, P. A. 2006, *ApJ*, 649, 498
- Dorch, S. B. F., Gudiksen, B. V., Abbett, W. P., & Nordlund, Å 2001, *A&A*, 380, 734
- Durney, B. R. 1995, *Sol. Phys.*, 160, 213
- Eddy, J. A. 1976, *Science*, 192, 1189
- Fan, Y. 2004, *Liv. Rev. Sol. Phys.*, 1, 1
- Fan, Y. 2008, *ApJ*, 676, 680
- Fan, Y., Fisher, G. H., & McClymont, A. N. 1994, *ApJ*, 436, 907
- Fan, Y., Abbett, W. P., & Fisher, G. H. 2003, *ApJ*, 582, 1206
- Gilman, P. A. 1983, *ApJs*, 53, 243
- Glatzmaier, G. A. 1987, *The Internal Solar Angular Velocity*, ed. B. R. Durney, & S. Sofia (Dordrecht: D. Reidel), 263
- Hoyng, P. 1988, *ApJ*, 332, 857
- Hoyt, D. V., & Schatten, K. H. 1998, *Sol. Phys.*, 181, 491
- Jones, C. A., Weiss, N. O., & Cattaneo, F. 1985, *Phys. D Nonlinear Phenomena*, 14, 161
- Jouve, L., & Brun, A. S. 2007, *A&A*, 474, 239
- Jouve, L., Brun, A. S., Arlt, R., et al. 2008, *A&A*, 483, 949
- Jouve, L., Brun, A. S., Arlt, R., et al. 2009, *ApJ*, 701, 1300
- Knobloch, E., & Weiss, N. O. 1983, *Phys. D Nonlinear Phenomena*, 9, 379
- Knobloch, E., Tobias, S. M., & Weiss, N. O. 1998, *MNRAS*, 297, 1123
- Krause, F., & Rädler, K. H. 1980, *Mean Field Magnetohydrodynamics and Dynamo Theory*, (Oxford: Pergamon Press)
- Lean, J. 2005, *Physics Today*, 58, 060000
- Leighton, R. B. 1969, *ApJ*, 156, 1
- Magara, T. 2004, *ApJ*, 605, 480
- Martínez-Sykora, J., Hansteen, V., & Carlsson, M. 2008, *ApJ*, 679, 871
- Miesch, M. S. 2005, *Liv. Rev. Sol. Phys.*, 2, 1
- Miesch, M. S., Elliott, J. R., Toomre, J., et al. 2000, *ApJ*, 532, 593
- Moore, D. R., Toomre, J., Knobloch, E., & Weiss, N. O. 1983, *Nature*, 303, 663
- Moss, D., & Brooke, J. 2000, *MNRAS*, 315, 521
- Nandy, D., & Choudhuri, A. R. 2001, *ApJ*, 551, 576
- Nandy, D., & Choudhuri, A. R. 2002, *Science*, 296, 1671
- Ossendrijver, A. J. H., & Hoyng, P. 1996, *A&A*, 313, 959
- Parker, E. N. 1955, *ApJ*, 121, 491
- Proctor, M. R. E. 1977, *J. Fluid Mech.*, 80, 769
- Roberts, P. H. 1972, *Phil. Trans. R. Soc. London*, 272, 663
- Rempel, M. 2006, *ApJ*, 647, 662
- Sparrow, C. T. 1982, *The Lorenz equations: Bifurcations, Chaos and Strange Attractors* (Berlin: Springer)
- Steenbeck, M., & Krause, F. 1969, *Astron. Nachr.*, 291, 49
- Stix, M. 1976, *A&A*, 47, 243
- Weiss, N. O., & Tobias, S. M. 2000, *Space Sci. Rev.*, 94, 99
- Tobias, S. M. 1997, *A&A*, 322, 1007
- Wang, Y.-M., Sheeley, N. R., Jr., & Nash, A. G. 1991, *ApJ*, 383, 431
- Weiss, N. O., Cattaneo, F., & Jones, C. A. 1984, *Geophys. Astrophys. Fluid Dyn.*, 30, 305
- Wilmot-Smith, A. L., Nandy, D., Hornig, G., & Martens, P. C. H. 2006, *ApJ*, 652, 696
- Yoshimura, H. 1978, *ApJ*, 226, 706